Chemical expansion due to hydration of proton conducting perovskite oxide ceramics

Annika K. Eriksson Andersson[1], Sverre M. Selbach[1],

Christopher S. Knee[2] and Tor Grande[1,*]

[1]*Department of Materials Science and Engineering, Norwegian University of Science and Technology, NO-7491 Trondheim, Norway*

[2] *Department of Chemical and Biological Engineering, Chalmers University of Technology, SE-412 96 Göteborg, Sweden*

Abstract

The crystal structures of proton conducting $BaZr_{1-x}Y_xO_{3-x/2}$ (BZY05-BZY20) and $BaCe_{0.8}Y_{0.2}O_{2.9}$ (BCY20) during hydration/dehydration has been studied by *in situ* high temperature X-ray diffraction and thermal analysis. A contraction / expansion of the crystal lattice associated with dehydration / hydration was observed for all materials at elevated temperatures and the polymorphic phase transition temperatures of $BaCe_{0.8}Y_{0.2}O_{2.9}$ were depressed by lowering the vapour pressure of water. A thermodynamic formalism is introduced to describe the *chemical expansion* associated with the hydration of oxygen vacancies in acceptor doped oxides. A conventional point defect model was applied to describe the lattice strain associated with the hydration. The chemical expansion is discussed with respect to the available volumetric data on the hydration of proton conducting oxide materials and its likely impact on ceramic fuel cells / hydrogen separation membranes utilising a proton conducting electrolyte.

---

[*] Corresponding author: grande@ntnu.no

Introduction

Proton conducting oxides have the unique property that hydrogen can be transported with high selectivity due to ionic conduction of protons. Oxides showing high proton conductivity and low electronic conductivity are attractive electrolyte materials in solid oxide fuel cells [1-3], while materials possessing both proton and electronic conductivity are potential membrane materials for separation of hydrogen from gas mixtures [4]. The latter is one of the most interesting technologies for production of hydrogen from fossil fuels or for pre-combustion CO_2 capture.

Acceptor doped cerates or zirconates, i.e $BaCe_{1-x}Y_xO_{3-x/2}$ and $BaZr_{1-x}Y_xO_{3-x/2}$, are currently the most promising proton conducting oxides [2, 5, 6], but questions have been raised concerning the chemical and mechanical stability of these materials [2]. The poor chemical stability can be explained by the high alkali earth content, which results in high reactivity towards acidic molecules like CO_2 [7, 8]. A rationale for the poor mechanical performance of the materials is still lacking. Chemically induced mechanical stress is anticipated by the considerable volume change during hydration/dehydration in proton conducting materials, see for example [9, 2].

The high proton conductivity in these oxides is facilitated by hydration of oxygen vacancies in oxide materials [2]

$$H_2O(g) + V_O^{\bullet\bullet} + O_O^x = 2OH_O^\bullet \tag{1}$$

where the Kröger-Vink notation is used to describe an oxygen vacancy ($V_O^{\bullet\bullet}$), oxygen ions at an oxygen lattice site (O_O^x) and hydroxide ions on an oxygen site ($OH_O^\bullet$). The concentration of oxygen vacancies is conventionally tailored by acceptor doping, i.e. typically rare earth substitution at the B-site of a perovskite, and the charge carrier (protons) concentration is controlled by the degree of hydration, reaction (1). A considerable volume expansion due to the hydration reaction was originally pointed out by Kreuer [2], but the phenomenology of this characteristic physical behaviour of proton conducting perovskite has so far not been described in detail. A recent study has clearly shown that hydration results in a volume expansion of the lattice for $BaZr_{1-x}Y_xO_{3-x/2}$ samples sintered at $T \geq 1500\,°C$ [9].

Point defect equilibria resulting in similar volume changes are well known for electroceramics with mixed valence state transition metals [10-19]. The volume change

associated with reduction of the oxidation state of the transition metal and increasing oxygen vacancy concentration has been defined as *chemical expansion* by Adler [10]. Chemical expansion is known to induce strain in electroceramics when exposed to a gradient in partial pressure of oxygen which can cause micro-cracking of, for example, dense electrolyte layers in SOFCs or partial oxidation membrane reactors [11].

Here we report on a high temperature X-ray diffraction investigation of the proton conducting oxides $BaCe_{0.8}Y_{0.2}O_{2.9}$ and $BaZr_{1-x}Y_xO_{3-x/2}$ (x = 0.05, 0.1, 0.2). The volume expansion/contraction associated with hydration/dehydration of these oxide materials in humid atmosphere is demonstrated, and the chemical expansion due to the hydration of oxide materials is presented in analogy with the definition of chemical expansion previously suggested by Adler [10]. A short review of available volumetric data of hydration of oxide materials is provided, and possible explanation for the expansion/contraction phenomenon is discussed.

Experimental

Ceramic powders with composition $BaZr_{1-x}Y_xO_{3-x/2}$ (x = 0.05, 0.1, 0.2, denoted as BZY05, BZY10 and BZY20) and $BaCe_{0.8}Y_{0.2}O_{2.9}$ (BCY20) were prepared via the aqueous nitric solutions spray pyrolysis method (Cerpotech AS, Trondheim, Norway). The as-pyrolysed BZY05 and BZY10 powders were calcined at 1673 K in air for 6 h and BZY20 at 1773 K for 12 h. The as-pyrolysed BCY20 powder was calcined at 1473 K in air for 12 h to remove traces of $BaCO_3$ and obtain a single phase powder according to powder X-ray diffraction. The calcined BCY20 powder was hydrated at 863 K for 48 h in humidified air (air bubbled through boiling water). The calcined BZY-powders were hydrated with a 5 K/min cooling rate from 1073 K to 423 K in the same atmosphere as BCY20. The humidity (pH_2O) of the atmosphere was not determined.

Ambient temperature powder X-ray diffraction (XRD) was collected on a Bruker AXS D8 Focus instrument (Cu K_α radiation) equipped with a Lynxeye[TM] detector to check phase purity. High temperature XRD (HT-XRD) data was collected with a θ-θ Bruker AXS D8 Advance (Cu K_α), mri Physicalische Geräte Gmb high temperature stage and VÅNTEC-1 position sensitive detector. The hydrated powder samples were placed on a Pt-strip heater and data were collected on heating in 25 K steps, (T = RT, 373-1123 K, 20°- 85° 2θ, step size

0.016°, step time 1 s) in flowing synthetic air (~1 ppm H_2O). A 300 s dwell time was set for each new temperature in order to equilibrate the sample. The temperature was measured by a S-type thermocouple welded to the Pt-strip and the estimated temperature uncertainty was ±5 K.

A dehydrated material was prepared by heating the hydrated powder *in situ* under vacuum (10^{-1} mbar) at 1073 K for 3 h in an alumina crucible using a radiant heater (BCY20) or a Pt-strip (BZY05, 10 and 20). X-ray diffraction patterns were collected on cooling from 20° to 75° 2θ from 1073 K to RT with 25 K steps. A 300 s dwell time was again used for equilibration. An S-type thermocouple mounted in close proximity to the sample (~1 mm from the sample edge) was used for temperature determination. Calibration of this system against an Al_2O_3 standard gave an estimated temperature error <15 K in flowing synthetic air. A significant error in the temperature measurement was observed for the cooling experiments performed in vacuum, and an internal standard of CeO_2 ($Fm\overline{3}m$ a = 5.412(3) Å at RT and a = 5.466(2) Å at 844K) was applied to reduce the error in the temperature measurements. The data between 538 K and ambient are not reported due to the significant error in the measured temperature.

Rietveld analysis of the XRD patterns were carried out using the Rietveld refinement program TOPAS Academic V4.1[20] using starting model parameters according to Malavasi *et al*.[21] for the different polymorphs of BCY20.

Thermogravimetrical analysis (TGA) (Netzsch STA 449C) was carried out on the hydrated samples with heating rates of 5 K/min from RT to 1073 K in synthetic air flow (30 ml/min). Weight loss at relatively low temperature due to absorbed H_2O or CO_2 made it difficult to determine the degree of hydration. The samples were therefore preheated *in situ* in the TGA to 623 K to remove species absorbed at the surface before commencing the analysis.

Results

The water content of the BZY05, 10 and 20 and BCY20 powders annealed in humid atmosphere was determined by TGA. The weight loss, recalculated to the number of moles of water per formula unit perovskite, is shown in Fig. 1. The weight loss of BCY20 in the T range 450 – 1000 K was 0.105±0.05 moles, which is in good accord with the theoretical maximum value of 0.1 moles based on filling of oxygen vacancies, according to reaction (1).

BCY20 was therefore fully hydrated according to TGA. The corresponding loss of water of BZY20, BZY10 and BZY05 were measured to 0.045±0.05, 0.039±0.04 and 0.034±0.03 mole H_2O per formula unit respectively. This indicates that the BZY05 sample was fully hydrated, while the BZY10 and BZY20 materials were far from fully hydrated despite the heat treatment in humid atmosphere. The *in situ* preheating of the powders to 623 K prior to the TGA analysis may have caused loss of water dissolved in the bulk of the BZY materials, which means that the degree of hydration based on the TGA data may be underestimated, particularly for BZY10 and BZY20.

The XRD-patterns of the calcined and hydrated BZY05, 10 and 20 and BCY20 powders showed no secondary phases, but the ambient diffraction patterns were found to suffer from severe line broadening. Analyses by scanning electron microscopy (SEM) revealed a particle size distribution in the range 1-5 μm, and analysis of the full width half maximum (FWHM) for all diffraction lines exhibited similar values, which could indicate possible stresses in the materials due to inhomogeneous hydration of the grains. The stress is caused by the expansion of the unit cell volume upon hydration as we will see below. The inhomogeneous hydration caused difficulties in the analysis of the heating data of BZY20 powder. Therefore two cubic phases with slightly different unit cell parameters was inserted in the analysis of the heating data (RT-600K) and the reported results for the partly hydrated materials is based on the cubic phase with the largest scale factor (90% : 10%). For example at 373 K has the 90% phase a cell parameter a = 4.224(1) Å and the 10% phase a = 4.205(1) Å resp. Upon dehydrating (T< 600K) the diffraction pattern could be analyzed with one single cubic phase.

All the XRD patterns of BZY05, BZY10 and BZY20 could be analyzed using the cubic $Pm\bar{3}m$ space group, both during the heating and cooling cycles. The XRD patterns of the hydrated BZY20 on heating are displayed in Fig. 2. All the diffraction lines could be indexed to the cubic symmetry, and no other reflections could be observed except from the Pt heating strip. The volume of the cubic unit cell during heating and cooling is displayed for the three BZY materials in Fig. 3. A close to linear relationship between the unit cell volume and temperature is evident during cooling in vacuum. In contrast a contraction of the crystal lattice is evident for all the hydrated materials in a certain temperature region during heating in air. The contraction takes place in the temperature interval where dehydration of BZY materials has previously been reported [9, 2], and in the same region as the mass loss shown by the TGA data presented in Fig. 1. The unit cell volume of the hydrated BZY05, BZY10

and BZY20 materials at ambient temperature decreased from 74.6(1), 74.8(1) and 75.7(1) Å^3 to 74.1(1), 74.2(1) and 75.0(1) Å^3 respectively after cooling in vacuum. The volumetric data clearly show that the hydration reaction (1) induces a volume expansion in line with previous data for acceptor doped BaZrO$_3$-based materials. The thermal expansion coefficients (TEC) of the materials, see Table 1, were determined by linear fits to the volumetric data. TEC for the dry materials were determined by cooling in vacuum, while the corresponding values for the hydrated materials were determined on heating in the T interval 303 to 573 K. Hydration of the BZY materials induces a small reduction of the thermal expansion coefficient.

The evolution of the XRD patterns of the hydrated BCY20 powder during heating in air and cooling in vacuum is shown in Fig. 4a-b). BCY20 is cubic at high temperature, and the cubic hkl indices for the $Pm\bar{3}m$ space group are given for the pattern recorded at 973 K. At lower temperatures the symmetry is clearly reduced as evidenced by the splitting of the diffraction lines, particularly visible for the pseudo cubic (200) and (211) reflections. BaCe$_{1-x}$Y$_x$O$_{3-x/2}$ (x = 0.0 – 0.2) at ambient temperature has been described previously with orthorhombic (*Pnma* No. 62, a = a$_p$√2, b = a$_p$/2, c = a$_p$√2) [22, 23] or monoclinic (*I2/m* No. 12, a ≈ a$_p$√2, b ≈ a$_p$/2, c ≈ a$_p$√2 and β ≠ 90) [21, 24] structures. Both space groups were applied to the ambient temperature diffraction pattern of hydrated BCY20 and the best Pawley fit was obtained for the monoclinic symmetry. The *I2/m* model was therefore used in the Rietveld analysis of the data collected on heating from RT to 623 K resulting in a satisfactory fit to the XRD data.

The splitting of the pseudo cubic (200) peak disappeared above 648 K and the monoclinic symmetry was no longer applicable. The orthorhombic *Imma* symmetry [25, 21] was used in the range 773 – 848 K. The peak broadening observed between ambient and 748 K diminished strongly at higher temperatures, giving sharper diffraction lines. The rhombohedral space group $R\bar{3}c$ (a ≈ a$_p$√2 and c ≈ a$_p$√12) was used between 773 and 848 K, where the weak single reflection at 33.5° 2θ could be indexed as the (113) reflection. Finally, peak splitting and the (113) reflection vanished and the diffractograms were analysed using the cubic ($Pm\bar{3}m$) space group in the temperature range 873-1123 K. The evolution of the different polymorphs and the pseudo cubic cell parameters is shown in Fig. 5a) and refined structural parameters are given in Table 2.

XRD patterns of BCY20 recorded during cooling in vacuum are shown in Fig. 4b). These XRD patterns could be refined using either $Pm\bar{3}m$ or $R\bar{3}c$ in the range 1073-639 K,

6

yielding similar agreement between the observed and calculated diffractograms. The (113) reflection associated with the $R\bar{3}c$ structure could be observed at 748 K and $R\bar{3}c$ gave the best fit to the data from 748 K to 639 K. In this interval there is no significant change in the peak shape and the $R\bar{3}c$ (113) reflection was relatively weak. No new super-reflections appeared upon cooling from 639 to 538 K, but the diffraction lines gradually broadened, with shoulders at 40.8° and 67.1° 2θ. The best fit for these patterns were obtained with the *Imma* structure. The evolution of the lattice parameters of the different polymorphs and the pseudo-cubic lattice parameter during cooling is shown in Fig. 5b) and refined parameters are given in Table 3.

The pseudo cubic unit cell volume of BCY20 determined during the heating cycle is plotted as function of temperature in Fig. 6. Initially a close to linear expansion of the volume is evident during heating, increasing from 85.43(1) $Å^3$ at 373 K to 86.35(1) $Å^3$ at 723 K. Thereafter the cell volume drops and at approximately 848 K the volume coincides with the volume observed during cooling in low vacuum. The relatively large reduction in the cell volume in this temperature range coincides with the mass loss observed by TGA (Fig. 1) and is again attributed to dehydration of the material [26]. The calculated thermal expansion coefficient (TEC) was estimated to $11.1 \cdot 10^{-5}$ K^{-1} for the hydrated material at low temperatures and $9.97 \cdot 10^{-6}$ K^{-1} for the dehydrated material at high temperatures (Table 1).

Discussion

Phenomenology of chemical expansion due to hydration

The thermal evolution of the unit cell volume (Fig. 3 and Fig. 6) demonstrates that the hydration of the oxide results in an expansion of the lattice for both type of oxide materials studied here. This is a general phenomenon which will occur in other oxide materials as well where hydration of oxygen vacancies occurs. The volume change associated with reaction (1) is a chemical expansion due to a change in the chemical composition. Chemical expansion has previously been introduced to describe the volumetric effect on a unit cell due to a change in chemical composition due to equilibration with the atmosphere. Chen and Adler [13] defined the isothermal and isobaric chemical expansion β_C as $\beta_C = \left(\partial \ln \hat{V} / \partial x \right)_{T,P}$, where $\hat{V}$ and *y* are the specific volume and a variable defining the chemical composition, respectively.

The effect of chemical expansion of the lattice parameter a can be expressed through the *chemical strain* $\varepsilon_C = (a - a_o)/a_o = (\Delta a/a_o)$, where a_o is the lattice parameter at the reference chemical composition. The *normalized chemical strain* [27] can be defined as $\varepsilon_C/\Delta y$ where $\Delta y = y - y_o$ and y_o is the reference chemical composition. Correspondingly, the *normalized chemical expansion* can be written as $3\varepsilon_C/\Delta y$. The defect equilibrium (1) expresses the hydration process, and we here define the compositional variable y. For $BaCe_{0.8}Y_{0.2}O_{2.9-y/2}(OH)_y$ (BCY20), y = 0.2 corresponds to a fully hydrated material, $BaCe_{0.8}Y_{0.2}O_{2.8}(OH)_{0.2}$, and y_o = 0 corresponds to the dehydrated reference composition $BaCe_{0.8}Y_{0.2}O_{2.9}$. The same approach was used for BZY05, BZY10 and BZY20. The normalized chemical strain and expansion caused by hydration reaction (1) is thus defined as $\varepsilon_C/\Delta y_{OH}$ and $3\varepsilon_C/\Delta y_{OH}$, respectively.

The chemical expansion of oxide materials due to hydration reaction (1) is compiled in Table 4. Chemical strain is either measured by X-ray (or neutron) diffraction or by dillatometry, and the change in water content has been determined by thermogravimetry as in this study. The chemical expansion is within the same order for all the perovskite materials, varying between 0.012 and 0.033, despite the variation in the crystal symmetry and chemical composition. Empirically, red-ox reactions in oxide materials have shown that materials with the same crystal structure seem to have similar chemical expansion values, suggesting that the volumetric effect of point defect equilibria are closely related to crystal structure [10, 11, 19]. We had initially anticipated that the dependence of the chemical expansion on the acceptor doping level in the BZY materials could be determined by the present data, but no clear dependence on the acceptor level in BZY could be found. Primarily this probably reflects the differing levels of hydration achieved for the BZY materials, and further investigations are therefore necessary to determine the compositional variation of the chemical expansion with respect to the acceptor doping level (initial oxygen vacancy concentration).

The significant expansion due to the hydration reaction (1) will induce a considerable stress as a proton conductor is hydrated. During hydration a compressional stress will be induced at the surface as vacancies are filled by larger hydroxide groups. The level of the stress will depend on the gradient in the concentration of the protons as they diffuse from the surface to the interior of a material. Correspondingly, a tensional stress is induced at the surface during dehydration. A tensional stress at surfaces is more critical than a

8

compressional stress [28], and we therefore would argue that chemical expansion in proton conductors is most critical with respect to mechanical failure due to dehydration during heating. The chemical expansion due to hydration is significant, and particularly in coarse grained ceramics chemically induced stress may induce micro-cracking, reduced mechanical strength and possibly catastrophic failure. Some of the problems with low mechanical performance of proton conducting oxides [2] may therefore be related to micro-cracking induced chemically by reaction (1.)

Modelling of the hydration/dehydration

We now turn our attention to a simple point defect model for the dependence of the molar volume (or unit cell volume) with respect to temperature and water content. The equilibrium constant for defect equilibrium (1) can expressed as

$$K = \frac{\left[OH_O^\bullet\right]^2}{\left[V_O^{\bullet\bullet}\right]\left[O_O^x\right]p_{H_2O}} = e^{-\frac{\Delta H_m}{RT} + \frac{\Delta S_m}{R}} \tag{2}$$

where $\left[OH_O^\bullet\right] = y$ as defined above, p_{H_2O} is the partial pressure of water and $\left[V_O^{\bullet\bullet}\right]$ and $\left[O_O^x\right]$ are the concentrations of oxygen vacancies and oxygen on oxygen lattice sites, respectively. ΔH_m and ΔS_m are the molar enthalpy and entropy of reaction (1), respectively. In the following we have used ΔH_m = -163.3 kJ/mol and ΔS_m = -167.9 J/molK for BCY20, while ΔH_m = -79.5 kJ/mol and ΔS_m = -88.9 J/molK were adopted for the BZY materials from [2]. Following Kreuer [2], with x = (0.05, 0.1 and 0.2) for BZY and x = $Y_{Ce}^\bullet$ = 0.2 for BCY20, the water content or $\left[OH_O^\bullet\right] = y$ is given by:

$$y = \frac{3Kp_{H_2O} - \sqrt{Kp_{H_2O}\left(9Kp_{H_2O} - x\left[6Kp_{H_2O} - 24\right] + x^2\left[Kp_{H_2O} - 4\right]\right)}}{Kp_{H_2O} - 4} \tag{3}$$

To model the volumetric effect of the chemical expansion upon hydration, we adopt to a large extent the ideas put forward in a model for the chemical expansion of fluorite type oxides [19]. We approximate the lattice parameter of the cubic perovskite as $a = 2\left(\bar{r}_B + \bar{r}_O\right)$ [19]. Here $\bar{r}_B = (1-x)r_{B_{B'}^x} + xr_{Y_{B'}'}$ where B' = Ce and Zr in BCY20 and the BZY materials, respectively, and $\bar{r}_O = (1/3)\left[\left((3-x/2) - y/2\right)r_{O_O^x} + (x/2 - y/2)r_{V_O^{\bullet\bullet}} + yr_{OH_O^\bullet}\right]$, where y is defined by eq. (3).

The ionic radii of Ce^{4+} (r = 0.87 CN = 6), Zr^{4+} (r = 0.72 Å CN = 6), Y^{3+} (r = 0.9 Å CN = 6), O^{2-} (r = 1.38 Å CN = 4) and OH^- (r = 1.35 Å CN = 4) were adopted from Shannon [29], while the oxygen vacancy radius, which is difficult to define, was empirically set to 1.18 Å to fit the experimentally observed chemical expansion. This value for the oxygen vacancy radius is close to that determined recently for ceria and zirconia based materials by a similar approach [19]. The structural deviation from a cubic perovskite was ignored in BCY20 for simplicity, but to fit the model to the data, and account for the structural distortion at low temperature, a renormalized cubic lattice parameter of $a_{o,300}$ = 4.396 Å was used for dry BCY20 at 300 K. Correspondingly 4.2155, 4.2017 and 4.1983 Å were used for BZY20, BZY10 and BZY05, respectively. Since reaction (1) does not involve changes in the oxidation state of the cations as is the case for chemical expansion due to redox equilibria [2], we have neglected the contribution due to the changes in the size of B-cation or change in the coordination of B due reaction (1). Finally the thermal expansion was included in the model by $a_{o,T} = a_{o,300} + \alpha T$, where α is the TEC reported in Table 1 for the dry material.

The modelled combined effects of thermal and chemical expansion for BCY20 with three different values of pH_2O is displayed together with the experimental unit cell volumes in Figure 6. With $pH_2O = 10^{-4}$ atm the model fits nicely to the data for the dehydration reaction in air. The temperature interval for the chemical contraction due to dehydration is shifted upward by increasing pH_2O in line with expectations. Values for pH_2O of $3 \cdot 10^{-7}$ fits the observed rehydration due to residual moisture in the XRD chamber upon cooling, while a value of 0.3 atm reproduces the volumes reported by Han et al. [31]. The corresponding model for the behaviour of the BZY materials is plotted together with the experimental unit cell volume in Figure 3. The experimentally observed dehydration is reproduced with the model for $pH_2O = 5 \cdot 10^{-5}$ atm. The model, based on equilibrium thermodynamics, predicts complete hydration of the materials in contrast to the experiments, where the materials were only partly hydrated.

Chemical expansion upon hydration/dehydration can thus, to a first approximation, be explained from the change in average ionic radii of the "anion" in the perovskite structure. As in the case of the volumetric effect of oxidation, further developments of the model can be derived by de-convoluting the individual contributions from the ionic species located at the oxygen lattice including the oxygen vacancy, oxygen anions and hydroxide anions.

Crystal structure and polymorphic phase transitions

The crystal structure evolution of the BZY materials is relatively simple as no structural phase transition take place. For a given BZY composition the cubic lattice parameter depends only on the temperature and degree of hydration (Fig. 3). Our intention was to start with fully hydrated BZY materials, but only part hydration of the BZY10 (78 % of theoretically available oxygen vacancies hydrated) and BZY20 (45 %) materials were obtained by the annealing procedure in the humid atmosphere used here. The contraction effect during dehydration was still evident, despite the incomplete degree of hydration. The data presented here are in qualitative agreement with previous data published for BZY and BZY materials [9, 2, 30]. Similar variable temperature X-ray diffraction data have been reported in the recent works by Wang *et al.* [30] on $BaCe_{0.7}Zr_{0.1}Y_{0.1}Yb_{0.1}O_{3-\delta}$, and Hiraiwa *et al.* [9] on $BaZr_{1-x}Y_xO_{3-x/2}$ ($0 \leq x \leq 0.25$). In the work of Hiraiwa *et al.* the hydration induced chemical expansion effects were only observed for samples sintered at either 1773 or 1873 K, while the powders heat treated at lower temperatures (1573-1673 K) did not exhibit the hydrated volume expansion. We surmise that these samples were not fully reacted as the cell parameters were significantly lower and, as such, the yttrium dopant did not act to create the oxygen vacancies required for hydration. Quantitative determination of the water content was not reported in [9], which makes quantitative comparison of the volume effect of hydration challenging.

The evolution of the lattice parameters and unit cell volume of BCY20 in heating, see Fig. 5 and 6, demonstrate clearly that the thermal evolution of the crystal symmetry and volume are strongly dependent on the degree of hydration. The hydrated sample displays three structural phase transitions on heating in flowing air (see Fig. 5); a 2nd order ($I2/m \rightarrow$ *Imma*) at approximately 630 K, a 1st order transition (*Imma* $\rightarrow R\bar{3}c$) at ~750 K, and finally a 2nd order phase transition ($R\bar{3}c \rightarrow Pm\bar{3}m$) at ~875 K. The data collected on cooling under low vacuum reveals shifts, by ~ 100 K, to lower T for the ($Pm\bar{3}m \rightarrow R\bar{3}c$) and ($R\bar{3}c \rightarrow$ *Imma*) transitions, and no strong evidence of the orthorhombic *Imma* structure reverting to a monoclinic *I*2/*m* structure of the initially hydrated phase was found on cooling back to RT. Since the degree of hydration will depend both on the temperature and the partial pressure of water, the structural phase transitions are expected to be shifted due to changes in the partial pressure of water. Malavasi *et al*. [21] and Han *et al.* [31] have reported previously on the thermal evolution of crystal structure of BCY20 based on neutron or X-ray diffraction data.

Malavasi *et al*. did not report any pronounced decrease in the unit cell volume upon heating, but these experiments were conducted in stagnant atmosphere where the sample was placed in a capsule. Assuming that the sample was initially fully hydrated (the water content was not reported) we infer that these experiments were conducted at a relatively high partial pressure of water since the sample generates its own humid atmosphere. The high phase transition temperatures reported by Malavasi et al. [21] are therefore reasonable. The work by Han *et al*. [31] has demonstrated clearly that the unit cell volume was significantly larger in wet atmosphere than in dry, which is in very good agreement with the present results. Unfortunately, quantitative comparison of the hydration reaction cannot be performed since the degree of hydration of the materials was not reported. The dehydration temperature of hydrated BCY20 reported by Han *et al*. [31] was significantly higher than observed here (pH$_2$O $\sim 10^{-4}$) due to their significantly higher partial pressure of water (pH$_2$O ~ 0.03 [31]), shifting reaction (1) to the right.

The situation for BCY20 is further complicated as the (de-)hydration reaction occurs within the same T interval as the structural transitions and small volume changes have been reported linked purely to the structural transitions [22]. Additionally an expansion of the cooling in vacuum data was observed in the interval 661-606 K which re-contracted again on further cooling. At present we do not understand the physical origin of this behaviour, but it may be related to the $R\bar{3}c \rightarrow Imma$ phase transition or systematic error in the temperature measurement at these relatively low temperatures.

Furthermore we note that the comparatively poor sensitivity of our XRD measurements to the phase transitions, that mainly reflect subtle re-organisations of the tilt patterns of the (Ce/Y)O$_6$ octahedra, introduces a level of uncertainty with the assignment of the phase transition temperatures. Nonetheless, comparing the data reported here and the work by Malavasi *et al*.[21], Ohzeki *et al*. [32] and Han *et al*. [31] we can confidently conclude that the phase transition temperatures are strongly shifted towards lower temperatures with decreasing degree of hydration. As already discussed the chemical expansion effects can, to a first approximation, be rationalized based on an increase in average anion size upon hydration and from simple tolerance factor arguments this is expected to destabilize the cubic aristotype. This prediction is consistent with the approx. 100 K shift seen here for the $Pm\bar{3}m$ to $R\bar{3}c$ transition (Fig. 5). Factors such as hydrogen bonding,

intimately linked to the proton transport mechanism, may also contribute to the more rapid lowering of symmetry observed for the hydrated sample.

Finally, it is also worth mentioning that not only thermodynamic factors but also the kinetics of the hydration/dehydration of the oxide materials is important for understanding of the thermal evolution of the crystal structure. Due to slow kinetics the materials may become only partly hydrated as in the case of the higher doped BZY materials investigated here, and with only part protonation an inhomogeneous water content distribution cannot be ruled out. Such inhomogeneous water distribution content may contribute to strain induced line broadening of diffraction reflections and reduce the quality of diffraction data. Since the structural phase transitions and the hydration / de-hydration coincide in the same temperature interval, kinetics may also play an important role in determining the crystal structure if sufficient equilibration time is not allowed. The most important factors influencing the kinetics of the hydration reaction are particle size (longer diffusion length), partial pressure of water and if stagnant atmosphere or flowing gas is used [18].

Conclusions

In summary, we have reported the crystal structure of the proton conducting $BaZr_{1-x}Y_xO_{3-x/2}$ and $BaCe_{0.8}Y_{0.2}O_{2.9}$ during hydration / dehydration measured by *in situ* high temperature X-ray diffraction. A contraction / expansion of the crystal lattice of all the materials was confirmed associated with hydration / dehydration at elevated temperatures. For BCY20 a clear dependence of the stability fields of the various crystal structures on the level of hydration of the material was also revealed. A thermodynamic formalism was introduced to describe the *chemical expansion* associated with the hydration reaction of oxygen vacancies in acceptor doped oxides. A conventional point defect model was applied to describe the lattice strain associated with the hydration reaction. The role of both thermodynamic and kinetic factors for the hydration/dehydration reaction has been addressed and the phenomenology of hydration in relation to functioning proton conducting ceramic membranes discussed. Finally, we note that an approach based on determining the hydration level via measurement of the magnitude of the unit cell expansion can offer advantages over the use of TGA data that is conventionally used. The interpretation of TGA data is often complicated by the presence of both chemically absorbed and surface adsorbed water in proton conducting materials.

Acknowledgements

References

[1] H. Iwahara, "Advanced ceramics for protonics", in *High Temperature Electrochemistry Ceramics and Metals*", Risø National Laboratory: Roskilde, 1996, 13-28.

[2] K. D. Kreuer, "Proton-conducting oxides," *Ann. Rev. Mater. Res.,* **33** 333-359 (2003)

[3] T. Norby, and Y. Larring, "Concentration and transport of protons in oxides," *Cur. Op. Solid State Mater. Sci.,* **2,** 593-599 (1997).

[4] T. Norby, and R. Haugsrud, *Nonporous Inorganic Membranes; Dense ceramic membranes for hydrogen separation*, Mundschau, WILEY-VCH Verlag, Weinheim, Germany, 2006.

[5] T. Schober, F. Krug, and W. Schilling, "Criteria for the application of high temperature proton conductors in SOFCs," *Solid State Ionics,* **97,** 369-373 (1997).

[6] B. Zhu, X. Liu, and T. Schober, "Novel hybrid conductors based on doped ceria and BCY20 for ITSOFC applications," *Electrochem. Comm.,* **6**, 378-383 (2004).

[7] K.H. Ryu, and S.M. Haile, "Chemical stability and proton conductivity of doped $BaCeO_3$-$BaZrO_3$ solid solutions," *Solid State Ionics,* **125**, 355-367 (1999)

[8] M.J. Scholten, J. Schoonman, J.C. van Miltenburg, and H.A.J. Oonk, "Synthesis of strontium and barium cerate and their reaction with carbon dioxide," *Solid State Ionics,* **61**, 83-91 (1993).

[9] C Hiraiwa, D. Han, A. Kuramitsu, A. Kuwabara, H. Takeuchi, M. Majima, and T. Uda, "Chemical Expansion and Change in Lattice Constant of Y-Doped $BaZrO_3$ by Hydration/Dehydration Reaction and Final Heat-Treating Temperature," *J. Am. Cer. Soc.,* **96**, 879-884 (2013).

[10] S.B. Adler, "Chemical Expansivity of Electrochemical Ceramics," *J. Am. Cer. Soc.,* 8**4**, 2117-2119 (2001).

[11] A. Atkinson, and T.M.G.M. Ramos, "Chemically-induced stresses in ceramic oxygen ion-conducting membranes," *Solid State Ionics,* **129**, 259-269 (2000).

[12] S.R. Bishop, T.S. Stefanik, and H.L. Tuller, "Defects and transport in $Pr_xCe_{1-x}O_{2-\delta}$: Composition trends," *J. Mater. Res.,* **27**, 2009-2016.

[13] Y. Chen, and S.B. Adler, "Thermal and Chemical Expansion of Sr-Doped Lanthanum Cobalt Oxide ($La_{1-x}Sr_xCoO_{3-d}$)," *Chem. Mater.,* **17**, 4537-4546 (2005).

[14] D. Chen, S.R. Bishop, and H.L. Tuller, "Praseodymium-cerium oxide thin film cathodes: Study of oxygen reduction reaction kinetics," *J. Electroceram.,* **28**, 62-69 (2012).

[15] X. Chen, and T. Grande, "Anisotropic and non-linear thermal and chemical expansion of $La_{1-x}Sr_xFeO_{3-\delta}$ (x = 0.3, 0.4, 0.5) perovskite materials," *Chem. Mater.* **25**, 3296-3306 (2013).

[16] X. Chen, and T. Grande, "Anisotropic chemical expansion of $La_{1-x}Sr_xCoO_{3-\delta}$," *Chem. Mater.,* **25**, 927-934 (2013).

[17] A. Fossdal, M. Menon, I. Wærnhus, K. Wiik, M.-A. Einarsrud, and T. Grande, "Crystal Structure and Thermal Expansion of $La_{1-x}Sr_xFeO_{3-\delta}$ Materials," *J. Am. Cer. Soc.,* **87**, 1952-1958 (2004).

[18]Grande, T., Tolchard, J.R. and Selbach, S.M., "Anisotropic thermal and chemical expansion in Sr-substituted LaMnO$_{3+\delta}$ - Implications for chemical strain relaxation," *Chem. Mater.,* **24**, 338-345 (2012).

[19]D. Marrocchelli, S.R. Bishop, H.L. Tuller, and B. Yildiz, "Understanding Chemical Expansion in Non-Stoichiometric Oxides: Ceria and Zirconia Case Studies," *Adv. Funct. Mater.,* **22**, 1958-1965 (2012).

[20]Coelho, A.A., *TOPAS Academic V4.1: General Profile and Structure Analysis Software for Powder Diffraction Data*. 1992-2007, Bruker AXS: Karlsruhe, Germany.

[21]L. Malavasi, C. Ritter, and G. Chiodelli, "Correlation between Thermal Properties, Electrical Conductivity, and Crystal Structure in the BaCe$_{0.80}$Y$_{0.20}$O$_{2.9}$ Proton Conductor," *Chem. Mater.,* **20**, 2343-2351 (2008).

[22]K S. Knight, "Structural phase transitions in BaCeO$_3$," *Solid State Ionics,* **74**, 109-117 (1994).

[23]KS. Knight, "Structural phase transitions, oxygen vacancy ordering and protonation in doped BaCeO$_3$: results from time-of-flight neutron powder diffraction investigations," *Solid State Ionics,* **145**, 275-294 (2001).

[24]K. Takeuchi, C.-K. Loong, J. W. Richardson Jr, J. Guan, S.E. Dorris, and U. Balachandran, "The crystal structures and phase transitions in Y-doped BaCeO$_3$: their dependence on Y concentration and hydrogen doping," *Solid State Ionics,* **138**, 69-77 (2000).

[25]C.S. Knee, A. Magraso, T. Norby, and R.I. Smith, "Structural transitions and conductivity of BaPrO$_3$ and BaPr$_{0.9}$Y$_{0.1}$O$_{3-d}$," *J. Mater. Chem.,* **19**, 3228-3247 (2009).

[26]A. K. Azad, and J.T.S. Irvine, "Location of Deuterium Positions in the Proton-Conducting Perovskite BaCe$_{0.4}$Zr$_{0.4}$Sc$_{0.2}$O$_{2.90}$·xD$_2$O by Neutron Powder Diffraction," *Chem. Mater.,* **21**, 215-222 (2009).

[27]H.L. Lein, K. Wiik, and T. Grande, "Thermal and chemical expansion of mixed conducting La$_{0.5}$Sr$_{0.5}$Fe$_{1-x}$Co$_x$O$_{3-d}$ materials," *Solid State Ionics,* **177**, 1795-1798 (2006).

[28]H.L. Lein, O.S. Andersen, P.E. Vullum, E. Lara-Curzio, R. Holmestad, M.-A. Einarsrud, and T. Grande, "Mechanical properties of mixed conducting La$_{0.5}$Sr$_{0.5}$Fe$_{1-x}$Co$_x$O$_{3-d}$ (0<x<1) materials," *J. Solid State Electrochem.,* **10**, 635-642 (2006).

[29]R. D. Shannon, "Revised Effective Ionic Radii and Systematic Studies of Interatomic Distances in Halides and Chalcogenides," *Acta Cryst.,* **A32** 751-767 (1976).

[30]S. Wang, F. Zhao, L. Zhang, and F. Chen, "Synthesis of BaCe$_{0.7}$Zr$_{0.1}$Y$_{0.1}$Yb$_{0.1}$O$_{3-d}$ proton conducting ceramic by a modified Pechini method," *Solid State Ionics,* **213**, 29-35 (2012).

[31]D. Han, M. Majima, and T. Uda, "Structure analysis of BaCe$_{0.8}$Y$_{0.2}$O$_{3-d}$ in dry and wet atmospheres by high-temperature X-ray diffraction measurement," *J. Solid State Chem.,* **205**, 122-128 (2013).

[32]T. Ohzeki, S. Hasegawa, M. Shimizu, and T. Hashimoto, "Analysis of phase transition behavior of BaCeO$_3$ with thermal analyses and high temperature X-ray diffraction," *Solid State Ionics,* **180**, 1034-1039 (2009).

[33]Y. Zhao, and D. Weidner, "Thermal expansion of SrZrO$_3$ and BaZrO$_3$ perovskites," *Phys. Chem. Miner.,* **18**, 294-301 (1991).

[34]F.G. Kinyanjui, S.T. Norberg, I. Ahmed, S.G. Eriksson, and S. Hull, "In-situ conductivity and hydration studies of proton conductors using neutron powder diffraction," *Solid State Ionics,* **225**, 312-316 (2012).

[35]S. Yamaguchi, and N. Yamada, "Thermal lattice expansion behavior of Yb-doped BaCeO$_3$," *Solid State Ionics,* **162-163**, 23-29 (2003).

[36]I. Sosnowska, R. Przenioslo, W. Schäfer, W. Kockelmann, R. Hempelmann, and K. Wysocki, "Possible deuterium positions in the high-temperature deuterated proton

conductor $Ba_3Ca_{1+y}Nb_{2-y}O_{9-d}$ studied by neutron and X-ray powder diffraction," *J. Alloys Comp.,* **328,** 226-230 (2001).

Tables

Table 1.

Thermal expansion coefficients values recorded in hydrated and dehydrated states for proton conducting perovskite oxides.

Material	TEC wet	TEC dry	Ref.
$BaCe_{0.8}Y_{0.2}O_{2.9}$	$11.1 \cdot 10^{-5}$	$9.94 \cdot 10^{-6}$	this work
$BaZr_{0.8}Y_{0.2}O_{2.9}$	$7.97 \cdot 10^{-6}$	$9.65 \cdot 10^{-6}$	this work
$BaZr_{0.9}Y_{0.1}O_{2.95}$	$7.40 \cdot 10^{-6}$	$8.80 \cdot 10^{-6}$	this work
$BaZr_{0.95}Y_{0.05}O_{2.997}$	$7.82 \cdot 10^{-6}$	$8.75 \cdot 10^{-6}$	this work
$BaCe_{0.7}Zr_{0.1}Y_{0.1}Yb_{0.1}O_{2.9}$	$9.91\text{-}9.98 \cdot 10^{-6}$		[30]
$BaZrO_3$	$20.6 \cdot 10^{-6}$		[33]
$BaZr_{0.85}Y_{0.15}O_{2.925}$	$8 \cdot 10^{-6}$		[2]

[3]Degree of hydration not specified.

Table 2.
Refined structural parameters for hydrated $BaCe_{0.8}Y_{0.2}O_{2.9}$ on heating in air at selected temperatures.

Space group , Temp	I2/m, 303K	Imma, 673K	R-3c, 823K	Pm-3m, 973K
a/Å	6.256(2)	6.268(2)	6.252(1)	4.425(1)
b/Å	8.741(3)	8.812(4)	6.252(1)	4.425(1)
c/Å	6.232(2)	6.249(2)	15.30(2)	4.425(1)
β(°)	90.910(2)	90	120	90
Vol./Å³	341.51(2)	345.18(2)	517.88(2)	86.67(1)
Ba	4i	4e	6b	1b
x	0.247(2)	0	0	0.5
y	0	0.25	0	0.5
z	0.751(2)	0.997(1)	0.25	0.5
Ce/Y	4e	4b	6a	1a
x	0.25	0	0	0
y	0.25	0	0	0
z	0.25	0.5	0	0
O(1)	4m	4e	18e	3d
x	0.140(4)	0	0.436(2)	0
y	0	0.25	0	0.5
z	0.246(5)	0.30(1)	0.25	0
O(2)	4g	8g		
x	0	0.25		
y	0.25(2)	0.514(3)		
z	0	0.25		
O(3)	4h			
x	0.5			
y	0.185(3)			
z	0			
Rwp(%)	8.98	8.82	9.13	9.98
Biso[4] (x 100 Å²)	1.40(1)	1.60(1)	2.00(1)	2.96(1)

[4] The same Biso parameter was used for all atoms.

Table 3.
Refined structural parameters for dehydrated $BaCe_{0.8}Y_{0.2}O_{2.9}$ on cooling in vacuum at selected temperatures.

| Space group, Temp	*Pm-3m*, 984K	*R-3c*, 749K	*Imma*, 625K	*Imma*, 303K
a/Å	4.426(1)	6.246(3)	6.252(4)	6.235(5)
b/Å	4.426(1)	6.246(3)	8.815(5)	8.758(1)
c/Å	4.426(1)	15.286(1)	6.240(4)	6.232(5)
Vol./Å^3	86.70(1)	516.44(9)	343.84(8)	340.31(3)
Ba	*1b*	*6b*	*4e*	*4e*
x	0.5	0	0	0
y	0.5	0	0.25	0.25
z	0.5	0.25	0.998(3)	0.993(2)
Ce/Y	*1a*	*6a*	*4b*	*4b*
x	0	0	0	0
y	0	0	0	0
z	0	0	0.5	0.5
O(1)	*3d*	*18e*	*4e*	*4e*
x	0	0.560(2)	0	0
y	0.5	0	0.25	0.25
z	0	0.25	0.448(3)	0.334(1)
O(2)			*8g*	*8g*
x			0.25	0.25
y			0.550(1)	0.515(9)
z			0.25	0.25
R$_{wp}$(%)	8.53	8.23	8.43	15.33
B$_{iso}$[4] (x 100 Å^2)	1.58(5)	1.29(4)	1.26(4)	0.29(1)

[4] The same B_{iso} parameter was used for all atoms.

Table 4.

Chemical expansion due to hydration of proton conducting ceramic oxides.

Material	ε_c	Δx	$\varepsilon_c / \Delta x$	Ref.	Method
$Ba(Zr_{0.85}Y_{0.15})O_{2.925}$	0.0040	0.15	0.027	[2]	dilatometry[5]
$Ba(Zr_{0.8075}Ce_{0.0425}Y_{0.15})O_3$	0.0022	0.15	0.015	[2]	dilatometry[5]
$BaIn_{0.5}Zr_{0.5}O_{2.75}$	0.0107	0.40	0.027	[34]	NPD[6]
$BaCe_{0.8}Yb_{0.2}O_{2.9}$	0.0031	0.20	0.016	[35]	dilatometry[5]
$Ba_3Nb_{1.82}Ca_{1.18}O_{8.73}$	0.0021	0.18	0.012	[36]	NPD
$BaCe_{0.8}Y_{0.2}O_{2.9}$	0.0052	0.26	0.02	this work	XRD
$BaZr_{0.95}Y_{0.05}O_{2.975}$	0.0015	0.08	0.019	this work	XRD
$BaZr_{0.9}Y_{0.1}O_{2.95}$	0.0015	0.10	0.015	this work	XRD
$BaZr_{0.8}Y_{0.2}O_{2.9}$	0.0034	0.104	0.033	this work	XRD

[5] Water content assumed to correspond to acceptor level

[6] Sample was bi-phasic, data presented here is based on the portion of the sample that hydrated/de-hydrated.
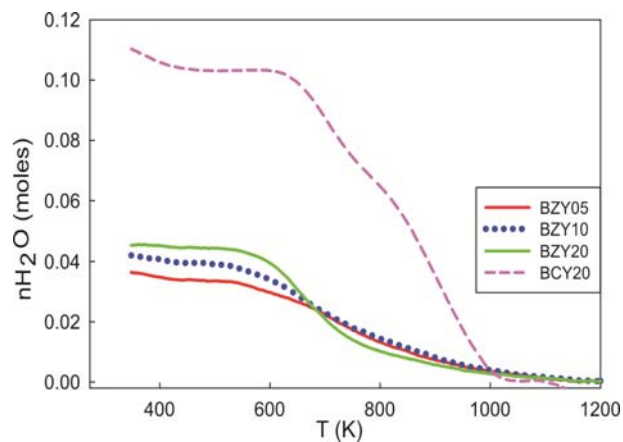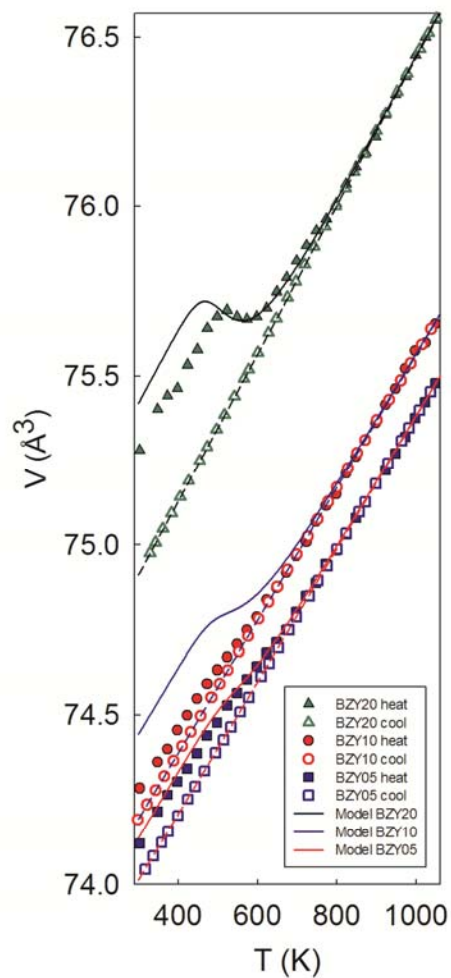
Figure 1.

Water content of the hydrated $BaZr_{1-x}Y_xO_{3-x/2}$ and $BaCe_{0.8}Y_{0.2}O_{2.9}$ materials. The weight loss due to dehydration of protons dissolved in to the crystal structure was estimated to be equivalent to 0.034 moles for BZY05, 0.039 moles for BZY10, 0.045 moles for BZY20 at 350 K and 0.103 moles for BCY20 at 450K.
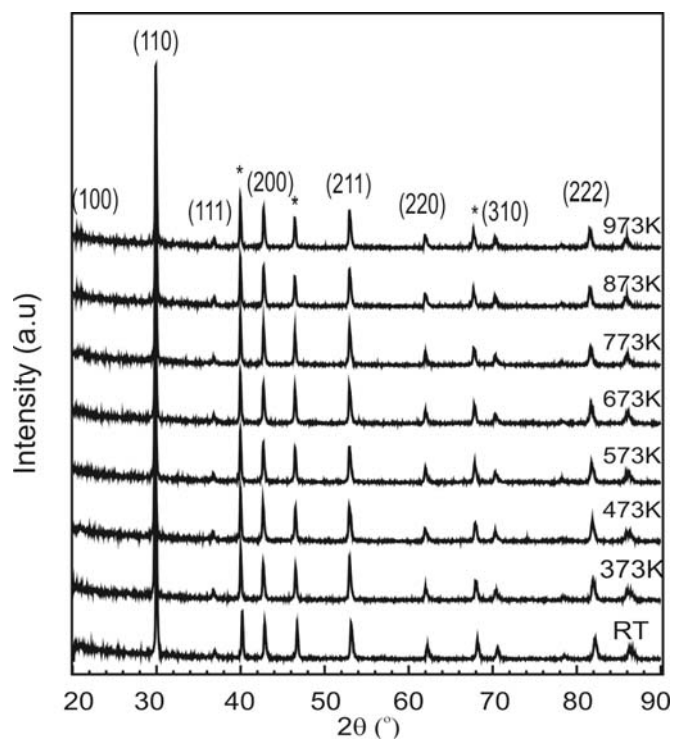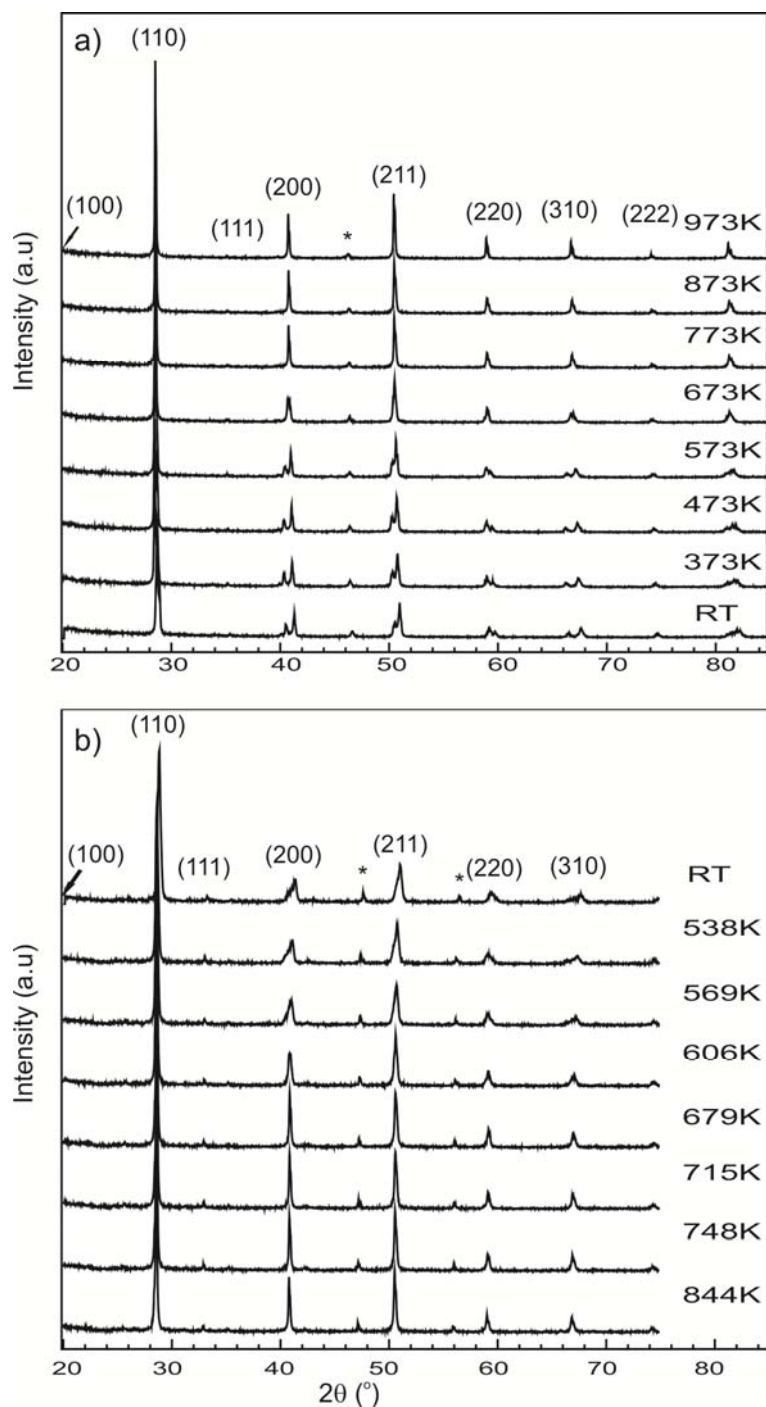

Figure 2.

XRD-plot as a function of temperature of hydrated BZY20 on heating in air. The stars indicate reflections contributed by the Pt-strip.
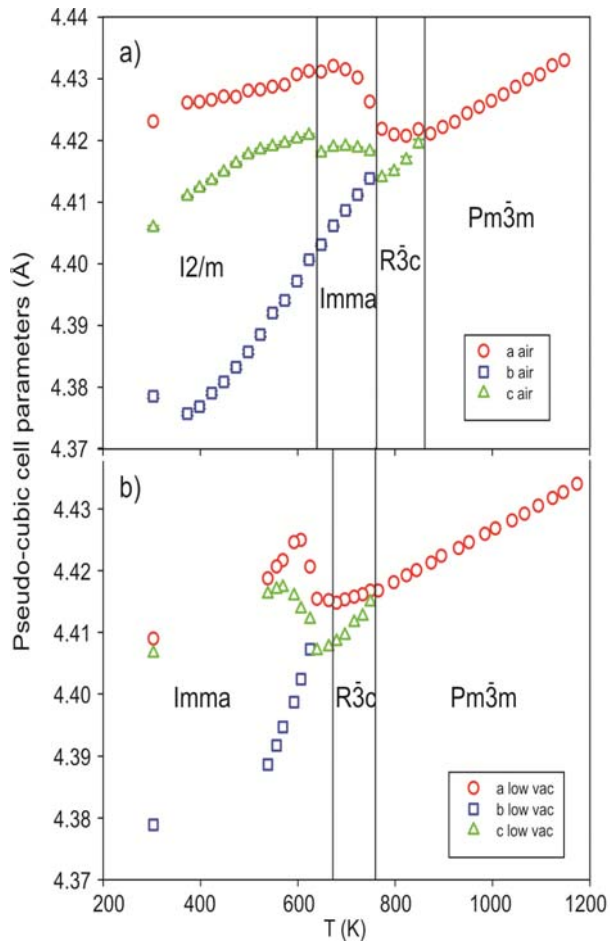
Figure 3.

Volumetric data of $BaZr_{1-x}Y_xO_{3-x/2}$, x = 0.05, 0.1 and 0.2 on heating in air and on cooling in low vacuum. The calculated cubic model of chemical expansion due to complete hydration and dehydration with $pH_2O = 5 \times 10^{-5}$ are shown by the solid lines. The x = 0.1 and 0.2 samples measured are not fully hydrated. The modeled volumes of dry materials with only thermal expansion are given by the dashed lines. Further details in relation to the model used for the calculated volumetric behavior are given in the discussion section.
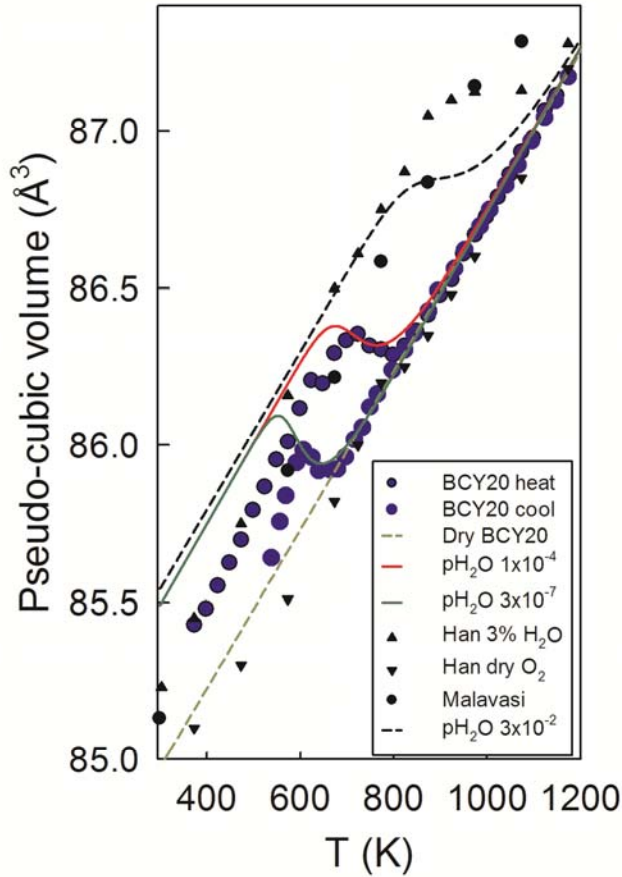
Figure 4.

XRD-plot as a function of temperature of a) hydrated BCY20 on heating in air, the star indicates a reflection contributed by the Pt-strip. b) de-hydrated BCY20 on cooling in low vacuum, the stars indicate reflection contributed by an internal standard CeO_2 ($Fm\overline{3}m$, a = 5.412(3) Å RT and a = 5.466(2) Å 844K.)

Figure 5.

a). Evolution of the different polymorphs and pseudo-cubic lattice parameters of a) BCY20 during heating in air and b) BCY20 during cooling in low vacuum. *I2/m* $a \approx c \approx \sqrt{2}a_p$ and $b \approx 2a_p$ *Imma* $a = c = \sqrt{2}a_p$ and $b = 2a_p$, $R\bar{3}c$ $a = \sqrt{2}a_p$ $c = \sqrt{12}a_p$.

Figure 6.

Pseudo cubic volumetric data BCY20 on heating in air and on cooling in low vacuum. The reference data Malavasi et al. [21] (open black circles) comes from neutron diffraction data collected on heating in static air in a silica glass container. The HTXRD data presented by Han et al. [31] was (open triangles (up)) collected on heating in a flow of O_2-3.12% H_2O and on cooling in dry O_2 (open triangles (down)). The calculated pseudo-cubic model of chemical expansion (combined with thermal expansion) at different pH_2O levels: 10^{-4} (solid red), $3 \cdot 10^{-7}$ (solid green) and $3 \cdot 10^{-2}$ (dashed black) atm are shown along with the thermal expansion (TEC) (dashed yellow). Further details in relation to the calculated volumetric behavior are given in the discussion section.